

Wind tunnel tests of 3D wind loads on tall buildings based on torsional motion-induced vibrations

Lianghao Zou^{1,2a}, Guoji Xu^{*2}, C.S. Cai^{2b} and Shuguo Liang^{1c}

¹School of civil engineering, Wuhan University, 299 bayi Road, Wuhan, 430072 China

²Department of Civil and Environmental Engineering, Louisiana State University, Baton Rouge, Louisiana 70803 USA

(Received January 26, 2016, Revised June 18, 2016, Accepted June 23, 2016)

Abstract. This paper presents the experimental results of the wind tunnel tests for three symmetric, rectangular, tall building models on a typical open terrain considering the torsional motion-induced vibrations. The time histories of the wind pressure on these models under different reduced wind speeds and torsional amplitudes are obtained through the multiple point synchronous scanning pressure technique. Thereafter, the characteristics of both the Root Mean Square (RMS) coefficients and the spectra of the base shear/torque in the along-wind, across-wind, and torsional directions, respectively, are discussed. The results show that the RMS coefficients of the base shear/torque vary in the three directions with both the reduced wind speeds and the torsional vibration amplitudes. The variation of the RMS coefficients in the along-wind direction results mainly from the change of the aerodynamic forces, but sometimes from aeroelastic effects induced by torsional vibration. However, the variations of the RMS coefficients in the across-wind and torsional directions are caused by more equal weights of both the aerodynamic forces and the aeroelastic effects. As such, for the typical tall buildings, the modification of the aerodynamic forces in the along-wind, across-wind, and torsional directions, respectively, and the aeroelastic effects in the across-wind and torsional directions should be considered. It is identified that the torsional vibration amplitudes and the reduced wind speeds are two significant parameters for the aerodynamic forces on the structures in the three directions.

Keywords: tall buildings; wind tunnel test; torsional motion-induced vibration; wind loads; aeroelastic effects

1. Introduction

Generally speaking, the governing factor in designing tall buildings is not the structure strength but the serviceability of the top floor (Islam *et al.* 1992). In other words, the acceleration response of the tall buildings under strong wind action is the decisive parameter for the structural wind-resistant design. The aerodynamic loads acting on the tall buildings are usually characterized

*Corresponding author, Ph.D., E-mail: gxu2@lsu.edu

^a Associate Professor, E-mail: lh Zhou@whu.edu.cn

^b Professor, E-mail: csc ai@lsu.edu

^c Professor, E-mail: liangsgwhu@sohu.com

as three dimensional (3D), namely, the dynamic forces in the along-wind and across-wind directions and the dynamic torque in the torsional direction (Solari 1985, Liang *et al.* 2002, 2004). In regard to the wind-induced vibrations, the displacement and acceleration responses near the peripheries of the cross-section at the top of the buildings can be significantly enlarged due to the torsional vibration of the structures, especially when the excited torsional frequency approaches the natural frequency of the structure in one certain translational axis. Therefore, the appropriate establishment of the 3D aerodynamic load models and the evaluation of aeroelastic effects are extremely significant in order to obtain reliable estimates of the wind-induced responses.

The main techniques to obtain the aerodynamic loads for tall buildings from wind tunnel tests are the multiple point synchronous scanning pressure (MPSSP) and the high frequency force balance (HFFB) techniques on the static rigid models. By applying the MPSSP technique, the mechanism and empirical model of 3D aerodynamic loads for tall buildings with typical side ratios of rectangular sections are proposed by Solari (1985), Cheung and Melbourne (1992), Kanda and Choi (1993) and Liang *et al.* (2002, 2004). In addition, Tamura *et al.* (1996) analyzed the fluctuating torsional moment coefficients, as well as the dynamic torsional responses for tall buildings. Later, for low and medium-rise buildings, the wind load combinations including the torsional effects were discussed by Tamura *et al.* (2008) and Keast *et al.* (2012). Isyumov and Case (2000) measured the wind-induced torsion with different aspect ratios on an open terrain exposure as modeled in the wind tunnel. Elsharawy *et al.* (2005, 2012, 2014) focused on the maximum torsion with the corresponding shear and maximum shear with the corresponding torsion for tall buildings. The HFFB technique is also commonly adopted in the design practice for obtaining aerodynamic loads for tall buildings. Using this technique in the wind tunnel, valuable test results for the aerodynamic loads on tall buildings with typical cross sections were proposed by Kareem (1992), Marukawa *et al.* (1992) and Gu and Quan (2004).

For the low and medium-rise buildings, the dynamic responses are dominated by the quasi-steady gust loadings with small resonant effects. Therefore, the structural vibration may not significantly influence the aerodynamic loads for a static rigid model in wind tunnel tests. However, more complicated results are expected for the high-rise and flexible buildings due to the significant vibration of these buildings under strong winds. When tall buildings oscillate under such strong wind actions, the dynamic wind pressure on their facades would be considerably distinctive as compared to the results for rigid structure models. In this regard, there are limited studies for effects of the structural vibration on the aerodynamic loads. This is one of the motivation for the current study.

In addition, it is expected that the aeroelastic effects, which significantly influence the response evaluation for tall buildings, may be prominent due to the structure oscillation under strong winds. The aeroelastic effects, especially the aerodynamic damping, in different directions were well discussed in the literature (Marukawa *et al.* 1996, Cheng *et al.* 2002, Gu and Quan 2004, 2005, 2014), where the empirical formulae of aerodynamic damping are proposed based on corresponding wind tunnel tests for single and/or multi-degree-freedom aeroelastic models. However, the vibration parameters such as amplitudes and frequencies of the aeroelastic model, which are the critical factors to determine the aeroelastic forces on the structures, can vary with the wind speeds in the wind tunnel. The effects of the vibration parameters on the aeroelastic forces are difficult to be accurately determined due to limited scenarios applied on the aeroelastic models. Therefore, updated test methods, single and bi-axial motion-induced vibration wind tunnel tests which can prescribe the vibration amplitudes and frequencies of the models in a single direction or two orthogonal directions in the wind tunnel by a specific device, were conducted to acquire the

aerodynamic forces and aeroelastic forces on tall building models. The mechanical difference of the two kinds of wind tunnel methods is that the model's vibration for the aeroelastic model wind tunnel test is induced by the wind loads, while the model's vibration for the motion-induced vibration wind tunnel test is induced by such a specific device and its amplitude remains constant with the change of wind speeds. Vickery and Steckley (1990, 1993) verified that the aerodynamic forces measured by the motion-induced vibration wind tunnel tests include the aeroelastic forces. The aeroelastic effects for the building models with different cross sections in the across-wind direction considering different vibration amplitudes, aspect ratios, and reduced wind speeds were then analyzed. In both of their wind tunnel tests, a sinusoidal vibration with the prescribed amplitudes and frequencies for the models under different wind speeds in the across-wind direction were considered by applying the single-axial motion-induced vibration devices. Based on the similar test method, Wu and Chang (2009) investigated the characteristics of the aerodynamic damping and aerodynamic stiffness for typical rectangular tall buildings in the along-wind direction with different wind speeds and frequencies. Thereafter Liang *et al.* (2011) discussed the effects of the structural vibration in the along-wind and across-wind directions (the bi-axial motion-induced vibrations) on the aerodynamic and aeroelastic forces. Different vibration amplitudes and frequencies in both the along-wind and across-wind directions were considered in his wind tunnel tests.

As a matter of fact, the torsional vibration was usually neglected in the wind tunnel tests for the single and bi-axial motion-induced vibration. Considering that the asymmetric wind pressures in the windward, leeward, and sideward facades can result in the torsional aerodynamic loads and hence the torsional vibration, in turn, would influence the aerodynamic and aeroelastic loads on the tall buildings in the along-wind and across-wind directions. This is another motivation for the current study.

For structurally asymmetric tall buildings, the intermodal coupling effects between the translational and torsional directions would occur among the wind-induced vibrations due to that the mass center, rigidity center, and geometry center for certain floors might not coincide with each other. As such, the statistical correlation and intermodal coupling effects were found to play significant roles in evaluating the wind induced responses for tall structures (Chen and Kareem 2005 and Chan *et al.* 2010). However, when buildings have the characteristics of symmetric shapes and mass center, they exhibit one-dimensional vibration such that the statistical correlation of the 3D dynamic wind loads does not make contributions to these responses and internal force in each direction (Liang *et al.* 2014). This indicates that the results of single-axial motion-induced vibrations in three directions could be reliable.

In summary, the aim of this paper is to investigate the impacts of torsional vibrations for tall buildings on the three dimensional structural aerodynamic loads and aeroelastic loads, where the buildings are characterized as symmetric rectangular shapes and their mass centers are coincident with resistance centers. At first, wind tunnel tests are conducted to measure the dynamic wind pressures on the prescribed building models. Meanwhile, torsional motion-induced vibrations with different amplitudes are considered. Then, the RMS coefficients and the spectra of the base shear/torque in the three directions are analyzed. Conclusions are finally presented.

2. Wind tunnel tests

The wind tunnel tests were carried out in the WD-1 boundary layer wind tunnel in Wuhan University, Wuhan, China. The wind tunnel is a horizontal direct-current type, low speed boundary layer wind tunnel with the cross section of 3.2 m (width) \times 2.1 m (height) \times 16 m (length). The test wind speed is adjustable continuously from 1 m/s to 30 m/s. Due to that the typical landform of tall buildings in the cities of China is Type C according to Chinese code (GB50009-2012 2012), the spire vortex generators and distributed rough cubic elements are adopted to realize the Type C turbulent wind field at a length scale of 1/400. Fig. 1 shows the profiles of the mean wind speed and turbulence intensities (I_u) at various heights over the test section. The longitudinal velocity spectrum of the generated boundary layer wind flow at a typical 0.6 m high agrees well with the Von-Karman type spectrum, as shown in Fig. 2. In Figs. 1 and 2, z is the height, V_z is the mean wind speed at the height z , n is the frequency, σ is the Root Mean Square of the longitudinal wind velocity, and $S_V(n)$ is the longitudinal wind velocity spectrum. The integral scales L_u^x of the longitudinal component of the turbulence in the along-wind direction range from 25 to 35 cm in the generated boundary layer.

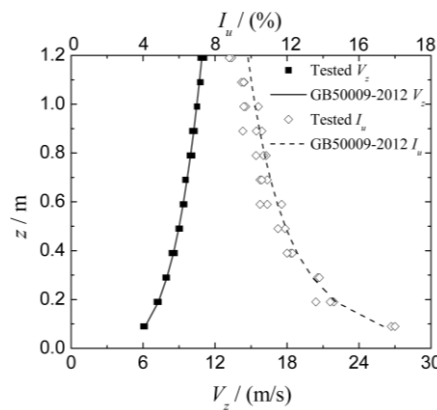


Fig. 1 Mean wind velocity and turbulence intensity profiles for open terrain exposure

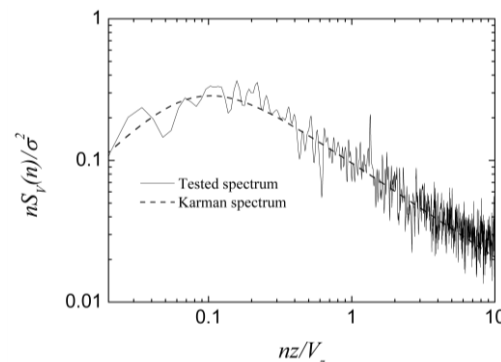


Fig. 2 Normalized wind speed spectrum

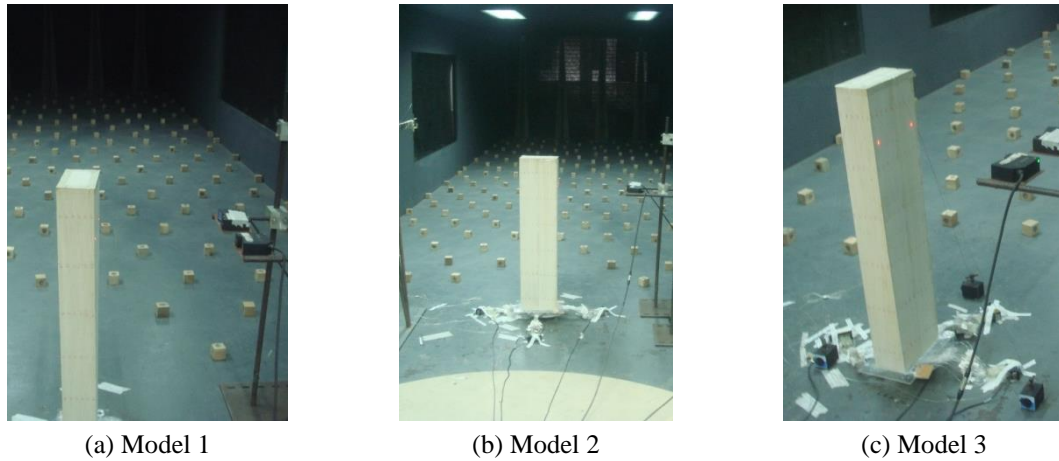
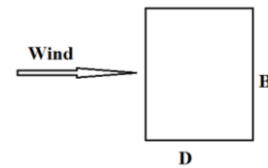


Fig. 3 Building models in wind tunnel

Table 1 Experimental building models

Models	Height/(m)	B×D/(m×m)	D/B
Model 1	0.9	0.15×0.15	1 : 1
Model 2	0.9	0.212×0.106	1 : 2
Model 3	0.9	0.106×0.212	2 : 1



Three tall building models (rectangular cross sections) with a geometric scale of 1:400 and three different side ratios, denoted as $D/B=1/2, 1$ and 2 , were considered, as shown in Table 1. The models have the same height (H) of 0.9 m and the same sectional area, $S = 0.0225 \text{ m}^2$. Therefore, they have the same aspect ratio, $H/\sqrt{S}=6$. The models were all made of balsa and can be deemed as rigid bodies due to their very high natural frequencies. During all the wind tunnel tests, the approaching flow was perpendicular to the side face B of the models. Fig. 3 shows the setup of the three models in the wind tunnel. Fluctuating wind pressures on the model's facades were measured with 192 pressure transducers placed at six different elevations throughout the height of the models, with 32 pressure transducers at each elevation, as shown in Fig. 4. During the measurement of the time histories of the wind pressures at the four facades, the Digital Temperature Compensation (DTC) net electronic pressure scanning valve system, made by American Pressure System Instrumentation (PSI) Scanning Valve Company, was used. In total three scanning valves were used to scan all the pressure signals. The sampling time of the fluctuating pressure was 120 s and the sampling frequency was 331 Hz. One cobra anemometer of Probe 100 series, produced by Australia Turbulent Flow Instrumentation (TFI) Company, was installed 1.0 m high in the left front of the model to measure the reference wind speed in the wind tunnel.

The tested models, representing typical tall buildings with a symmetric, rectangular cross section, were mounted on a device which was used to produce the torsional motion-induced

vibration excitations, as shown in Fig. 5. This device is a torsional motion-induced vibration device, where an eccentric wheel is driven by a direct-current motor and can rotate forcing the connecting rod to move forward and backward in a sinusoidal curve. The mechanism of this device is sketched in Fig. 6. The generated torsional vibrations will dominate the vibrations of the tested models in the wind tunnel through the connecting rod. The frequency and amplitude of the torsional vibration can be conveniently adjusted by a control system, which controls the rotational speed of the direct-current motor and the eccentricity of the wheel, respectively. Therefore, a sinusoidal vibration of the models in the torsional direction, which has a torsional fundamental constant type mode shape (Zhang *et al.* 1994, 1995) with a stable frequency and amplitude, can be realized by using this device. In order to obtain the amplitude of the models' torsional vibration with desirable accuracy in the wind tunnel tests, two displacement laser sensors were used to simultaneously measure the displacement histories for two rims on the same side and at the same height of the model. The sampling frequency was 500 Hz and the total sampling time was 120 s, the same as the sampling time for the fluctuating pressure.

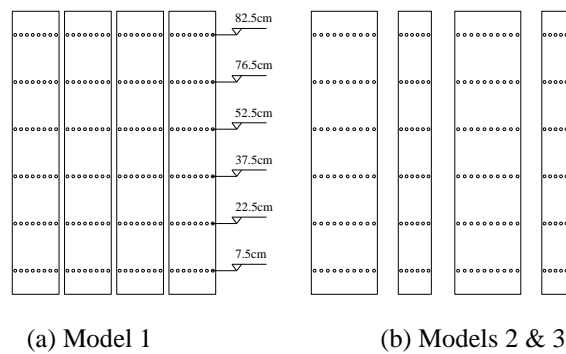


Fig. 4 Pressure taps on the models

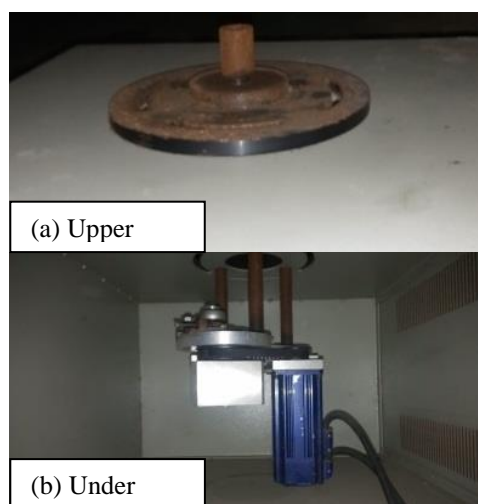


Fig. 5 Device photos for motion-induced vibration

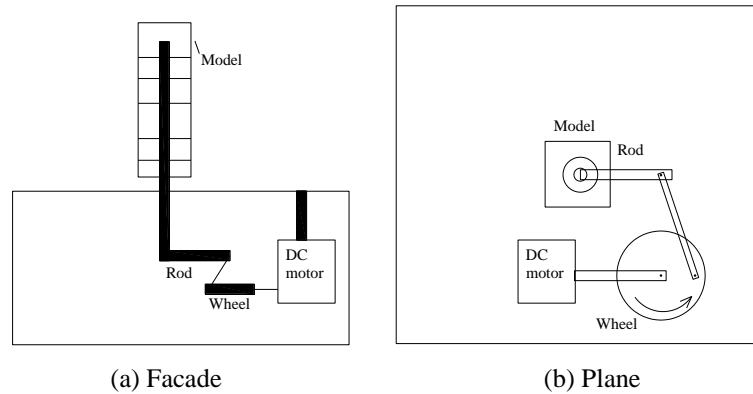


Fig. 6 Principal Structure of the torsional motion-induced vibration mechanism

As a matter of fact, due to the application of more flexible and ductile materials in the construction of tall buildings recently and in the future, the structural natural frequencies of super tall buildings in different directions decrease and the design reduced wind speed increases. As a result, the design wind speed would reach or exceed the vortex lock-in wind speed in the acrosswind direction even in the torsional direction, indicating that the vibration amplitude would increase sharply (Chen 2013). In order to analyze the effects of the high reduced wind speeds and large torsional amplitudes on the 3D wind loads of tall buildings, the torsional vibration frequency n_0 is set to be 6 Hz and the studied vibration amplitudes are set to be 0 rad (static rigid model), $\pi/90$ rad, $\pi/45$ rad, $\pi/30$ rad, and $\pi/22.5$ rad, respectively. The wind speeds at the top of the models, V_H , vary from case to case, ranging about from 3 to 15 m/s. The reduced wind speeds (V_H/n_0B) range about from 2 to 24 for the three models. In these cases, the torsional natural frequency is reasonably regarded as 0.15 Hz and the frequency scale is 40. Therefore, the wind speed scale is 1:10. This means the wind speed at the top of the buildings ranges from 40 m/s to 100 m/s. Although this wind speed seems to be relatively high for the prototype of the models in this paper, considering that the structures with the same cross section have the same wind flow characteristics under the same reduced wind speed, the wind speed at the top of the structures would decrease with the decrease of both the frequency and side face B . Therefore, for slender flexible structures with the low natural frequency, the wind speed at the top of the structures would reasonably fall in the range of scenarios tested in the present study.

3. Methodology of test data processing

In the wind tunnel tests, various wind speeds and torsional vibration amplitudes were considered to cover a large number of cases representing certain scenarios. However, the measured results need to be appropriately processed in order to obtain informative and straightforward observations. Based on the measurements of the time histories of the displacement for the rims and the wind pressure from the pressure transducers, the angular displacement histories of the models and RMS coefficients of the base shear (or the base torque) in the along-wind, across-wind, and

torsional directions were obtained by the following data processing.

Theoretically, the angular displacement of the torsional vibration can be derived as follows

$$d_t(i) = \frac{d_{p1}(i) - d_{p2}(i)}{L} \quad (1)$$

where, $d_{p1}(i)$ and $d_{p2}(i)$ are the displacements of the i -th sampling data measured by the two Laser sensors, respectively; L is the distance between the two measured points; and $d_t(i)$ is the corresponding angular displacement for the i -th sampling data. One typical sample of the vibration curve for the torsional motion-induced vibration of model 2 is demonstrated in Fig. 7, where a simple harmonic oscillation with a stable frequency and amplitude was obtained and V_H is the mean wind speed at the top of the models.

In order to evaluate the aerodynamic loads in the three directions, a coordinate system of the models is used for calculating these loads, as shown in Fig. 8. The time histories of the wind loads at each elevation in the along-wind (X-axis) and across-wind (Y-axis) directions can be derived using the superimposition of the wind pressures from each pressure transducer considering the appropriately weighted reduced area for each transducer. In addition, the torque at each elevation can be evaluated by superimposing the corresponding moments from each transducer at the four facades. Here, the center point of the horizontal cross section of the model is taken as the moment center.

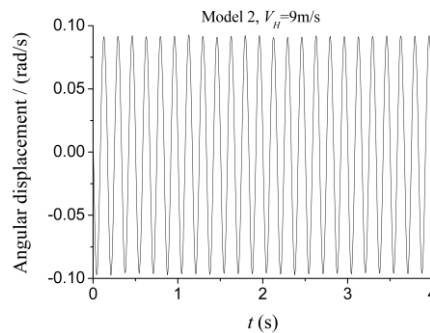


Fig. 7 Torsional motion-induced vibration curve

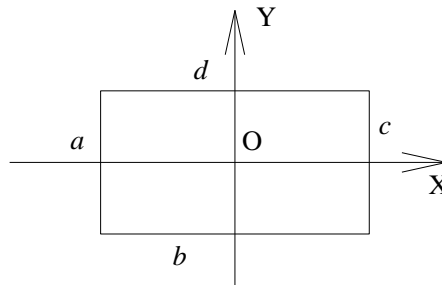


Fig. 8 The coordinate system of the models for calculation

The shear (or the torque) for the j -th elevation in the along-wind ($F_{Lj}(t)$), across-wind ($F_{Cj}(t)$), and torsional directions ($T_{Tj}(t)$), respectively, can be calculated as follows

$$F_{Lj}(t) = \sum_{i=1}^q w_{ji}^b(t) B_{ji}^b H_{ji}^b - \sum_{i=1}^s w_{ji}^d(t) B_{ji}^d H_{ji}^d \quad (2)$$

$$F_{Cj}(t) = \sum_{i=1}^p w_{ji}^a(t) B_{ji}^a H_{ji}^a - \sum_{i=1}^r w_{ji}^c(t) B_{ji}^c H_{ji}^c \quad (3)$$

$$T_{Tj}(t) = - \sum_{i=1}^q w_{ji}^b(t) B_{ji}^b H_{ji}^b Y_{ji}^b + \sum_{i=1}^s w_{ji}^d(t) B_{ji}^d H_{ji}^d Y_{ji}^d \\ + \sum_{i=1}^p w_{ji}^a(t) B_{ji}^a H_{ji}^a Y_{ji}^a - \sum_{i=1}^r w_{ji}^c(t) B_{ji}^c H_{ji}^c Y_{ji}^c \quad (4)$$

where, the superscripts ($N = a, b, c, d$) refer to the defined façades at each level of the model and there are p, q, r , and s pressure transducers in each façade, respectively; $w_{ji}^N(t)$ is the instantaneous wind pressure of the i -th pressure transducer at the j -th level in the N -th façade at the time t ; B_{ji}^N and H_{ji}^N are the reduced width and height for the i -th pressure transducer located at the j -th level in the N -th façade; X_{ji}^N and Y_{ji}^N are the coordinates of the corresponding pressure transducers. The base shear/torque in the three directions can be obtained by superimposing the shear (or the torque) at all elevations.

The RMS coefficients of the base shear/torque in the along-wind ($\mu_{\sigma L}$), across-wind ($\mu_{\sigma C}$), and torsional directions ($\mu_{\sigma T}$), respectively, can be calculated as follows

$$\mu_{\sigma L} = \frac{\sigma_{F_L}}{\rho V_H^2 S / 2} \quad (5)$$

$$\mu_{\sigma C} = \frac{\sigma_{F_C}}{\rho V_H^2 S / 2} \quad (6)$$

$$\mu_{\sigma T} = \frac{\sigma_{M_T}}{\rho V_H^2 S B / 2} \quad (7)$$

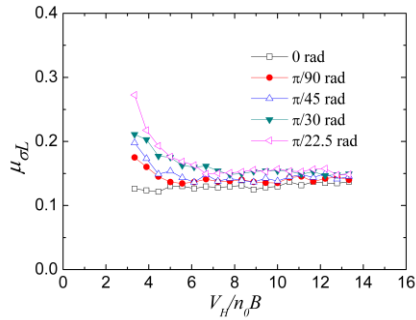
where, σ_{F_L} , σ_{F_C} and σ_{M_T} are the RMS of the base shear/torque in the along-wind, across-wind, and torsional directions, respectively; ρ is the air density.

4. The RMS coefficients of aerodynamic loads

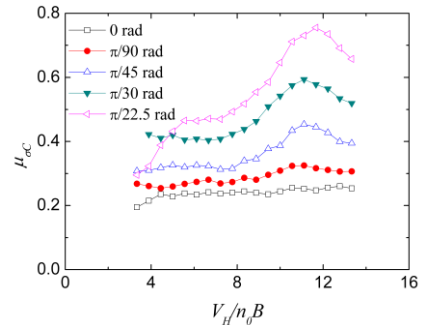
4.1 Analysis of the along-wind RMS base shear coefficients

Fig. 9 shows the RMS coefficients of the base shear in the along-wind direction versus the reduced wind speeds ($V_H/n_0 B$) considering various torsional amplitudes. It is noteworthy that: (1) generally speaking, the RMS coefficients of the base shear for the three models under different torsional amplitude conditions decrease with the increase of the reduced wind speeds. The RMS coefficients tend to remain at a constant value for the static rigid models (0 rad vibration amplitude). However, they tend to be larger for larger torsional vibration amplitudes, especially when the wind speed is relatively low. There are no significant differences between the results for different vibration amplitudes when the wind speed is relatively high; and (2) the effects of the

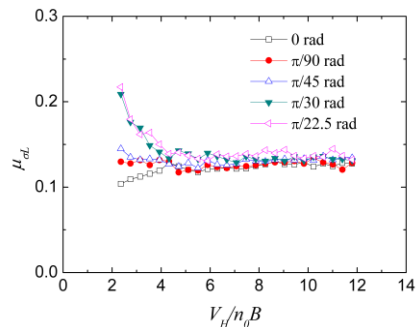
torsional vibration on the along-wind RMS coefficients of the base shear are more significant with larger side ratios of the models under high reduced wind speeds.



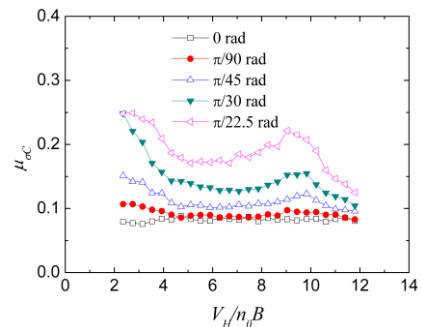
(a) Model 1



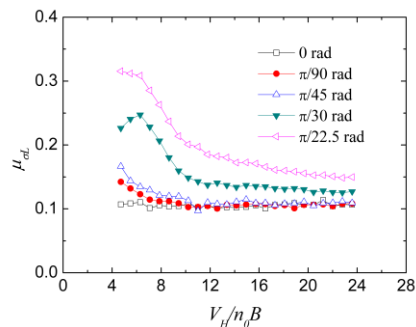
(a) Model 1



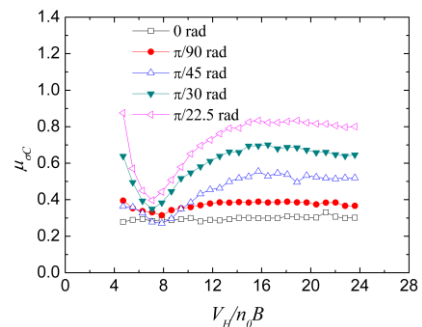
(b) Model 2



(b) Model 2



(c) Model 3



(c) Model 3

Fig. 9 RMS shear coefficients in the along-wind direction Fig. 10 RMS shear coefficients in the across-wind direction

4.2 Analysis of the across-wind RMS base shear coefficients

The RMS base shear coefficients of the three models in the across-wind direction are illustrated in Fig. 10. Though Fig. 10 shows that the RMS base shear coefficients in the across-wind direction notably increase with the increase of the amplitudes of the torsional vibration, the trends in the across-wind direction along with the reduced wind speeds are significantly different from the results in the along-wind direction. Generally speaking, the RMS base shear coefficients in across-wind direction have the characteristics of decreasing first, then increasing, and finally decreasing again, with the increase of the reduced wind speeds, especially for models 2 and 3. The coefficients reach a maximum under the critical wind speeds of vortex-excited resonance (the reduced wind speed approximately is 12, 10 and 14 for model 1, model 2 and model 3, respectively). Meanwhile, a significant decrease is observed when the reduced wind speeds exceed the critical wind speeds of vortex-excited resonance for model 1 and model 2, while the decrease is not significant for model 3.

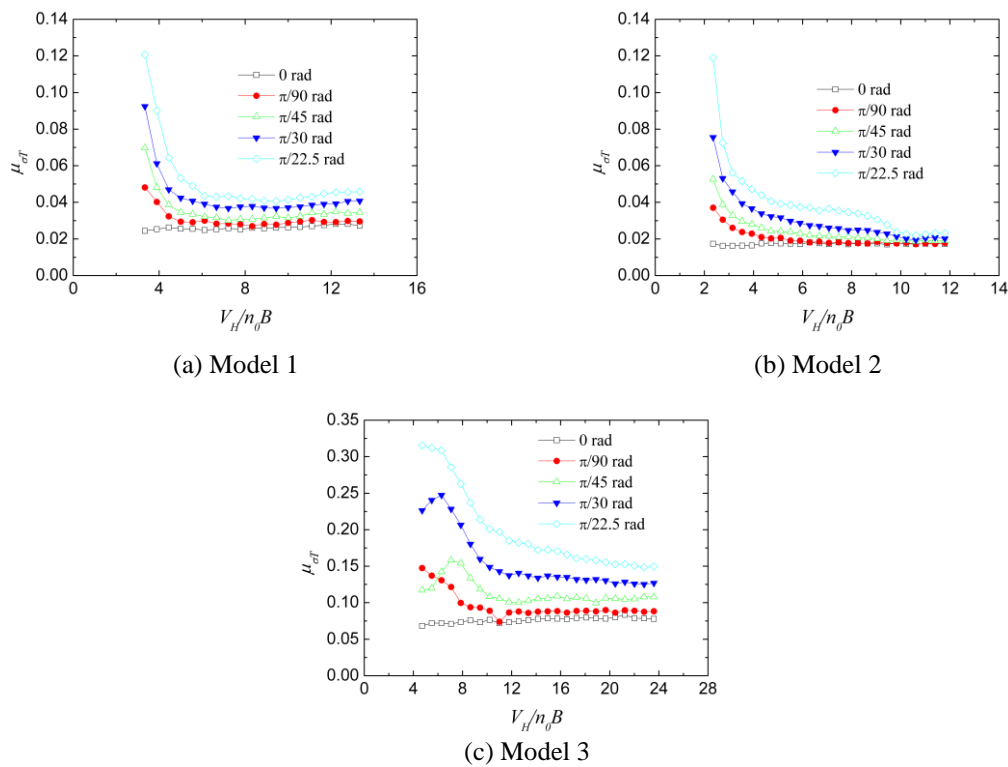


Fig. 11 RMS torque coefficients in torsional direction

4.3 Analysis of the torsional RMS base torque coefficients

Fig. 11 shows the results of the RMS torque coefficients in the torsional direction versus the reduced wind speeds under various amplitudes of the torsional vibration. It demonstrates that the RMS base torque coefficients in the torsional direction have similar variation trends as those in the along-wind direction: The RMS base torque coefficients in the torsional direction decrease with the increase of the reduced wind speeds and increase with the increasing amplitudes of the torsional vibration. Fig. 12 shows the ratios of the RMS coefficients under the condition of the $\pi/22.5$ rad amplitude to those of the 0 rad amplitude (the RMS coefficients of the $\pi/22.5$ rad amplitude divide by the results of the 0 rad amplitude) in the along-wind and torsional directions. It indicates that the influence of the torsional vibration to the RMS base torque coefficients in the torsional direction is more significant than that to the RMS base shear coefficients in the along-wind direction.

5. Analysis of the spectra of 3D dynamic wind loads

The dynamic wind loads, obtained by the torsional motion-induced vibration wind tunnel tests of the models, mainly contain two components: the aerodynamic forces and the aeroelastic forces (Vickery and Steckley 1990, 1993). The aerodynamic forces, induced by the wind action, can be measured by the wind tunnel tests on a static rigid model when the effect of the structural vibration is neglected. The aeroelastic forces, whose characteristic frequencies are essentially the same as the structural vibration frequencies, are induced by the coupling vibration of the structure and wind. Only analysing the RMS coefficients of the base shear/torque in three directions cannot acquire the details about the components of the structural aerodynamic loads. Therefore, it is necessary to investigate the spectra of the 3D aerodynamic loads of the models.

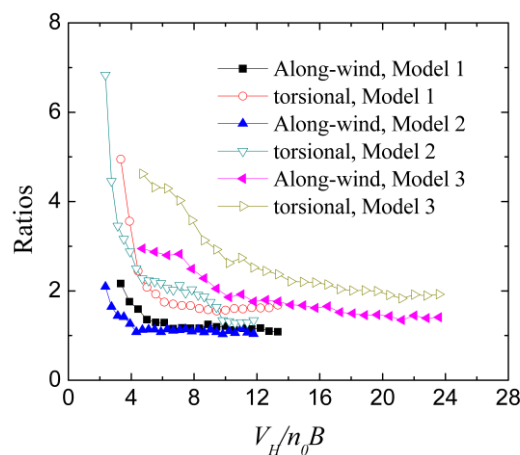


Fig. 12 the ratios of the RMS coefficients in along-wind and torsional directions

5.1 Along-wind base shear spectra

The influence of the torsional vibration amplitudes on the along-wind spectra of the base shear under various reduced wind speeds of the three models are shown in Figs. 13-15, respectively. The main observations for the along-wind spectra are as follows:

(1) The spectral peaks of the along-wind base shear spectra are located at a very lower reduced frequency, and gradually decline with the increase of the reduced frequency. This illustrates that the along-wind spectra has the typical turbulence characteristics.

(2) Hardly any spectral peaks can be found in the base shear spectra at the frequency (6 Hz) of torsional motion-induced vibration. This illustrates that the along-wind aeroelastic effects, induced by the torsional vibration, are very small and hence can be neglected.

5.2 Across-wind base shear spectra

Figs. 16-18 show that the across-wind spectra of the base shear change along with the reduced wind speeds and torsional vibration amplitudes for the three models, respectively. Discussions for the general observations of the across-wind spectra are as follows:

(1) Under the lower reduced wind speeds, two spectral peaks for the three models are found (i.e., Fig. 16(a)) and both of them have typical narrow-band characteristics. One spectral peak at the lower frequency is induced by the vortex shedding, where the characteristic reduced frequency is equal to the critical reduced frequency of the vortex. The other spectral peak, where the frequency is nearly equal to the torsional vibration frequency (6 Hz), is apparently motivated by the torsional vibration. This shows that the component of aeroelastic forces in the across-wind direction induced by the torsional vibration is very significant.

(2) The two spectral peaks increase significantly with the increase of the torsional amplitudes, while the bandwidths of the two spectral peaks do not change much.

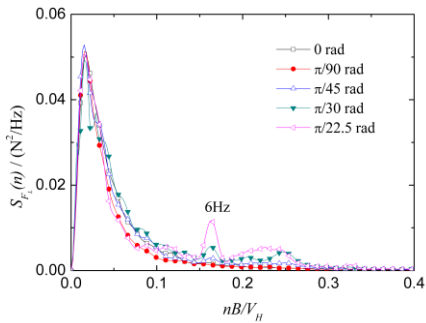
(3) When the test wind speeds increase to reach the critical wind speed of the vortex-induced resonance, the two spectral peaks combine into one sharp spectral peak with the narrow-band characteristics. In addition, the spectral peak value increases with the increase of torsional amplitude as shown in Figs. 16(b), 17(b), and 18(b). When the wind speeds increase to a certain level, there is also only one spectral peak at the torsional vibration frequency 6 Hz due to the lock-in of vortex shedding as shown in Figs. 16(c) and 18(c). When the reduced wind speeds are further increasing, the two spectral peaks appear again, and the frequency of the vortex shedding exceed the torsional vibration frequency as shown in Fig. 17(c).

5.3 Base torque spectra

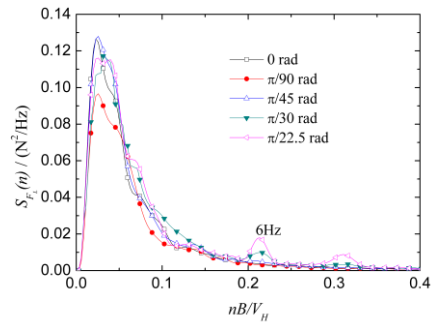
Figs. 19-21 show the base torque spectra of three different reduced wind speeds and different torsional vibration amplitudes in the torsional direction for the three models, respectively. It is observed that:

(1) There are two typical spectral peaks in the base torque spectra of the three models. The one at the lower frequency has the wide-band characteristics, and its component, representing the aerodynamic forces on the structures, is mainly induced by the aerodynamic forces in the torsional direction. The other spectral peak at the torsional vibration frequency 6 Hz has the typical narrow-band characteristics, which represents the aeroelastic effects on the structures, and is motivated by the torsional vibration.

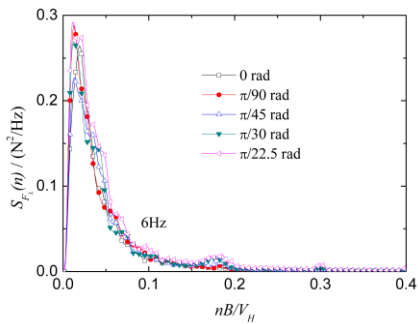
(2) With the increase of the reduced wind speeds, the spectral peak, representing the torsional aerodynamic forces, moves to a higher frequency. Then, it is superimposed with the spectral peak at the torsional vibration frequency.



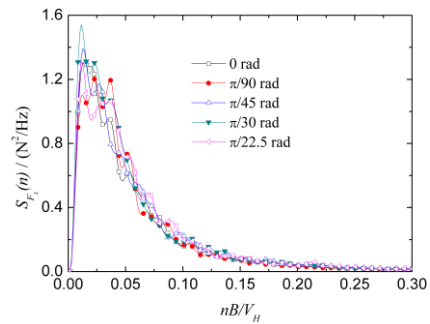
(a) $V_H/(n_0B)=5$



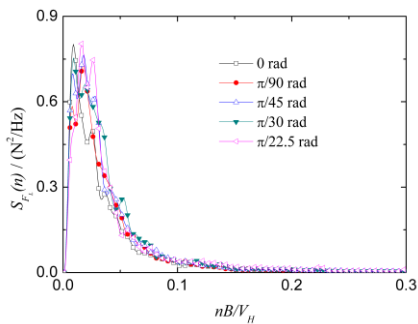
(a) $V_H/(n_0B)=4.7$



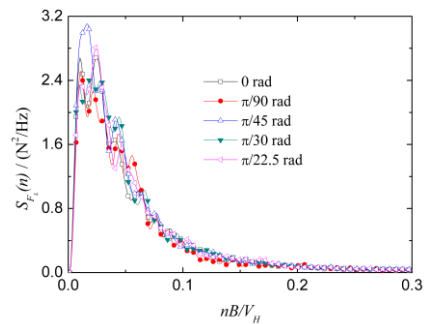
(b) $V_H/(n_0B)=10$



(b) $V_H/(n_0B)=9.4$



(c) $V_H/(n_0B)=13.3$

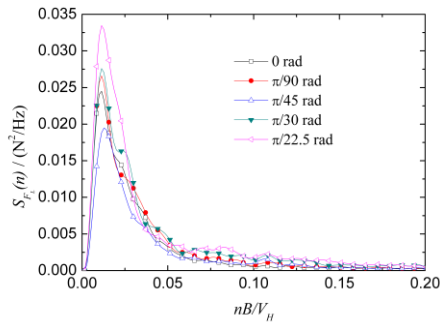


(c) $V_H/(n_0B)=11.8$

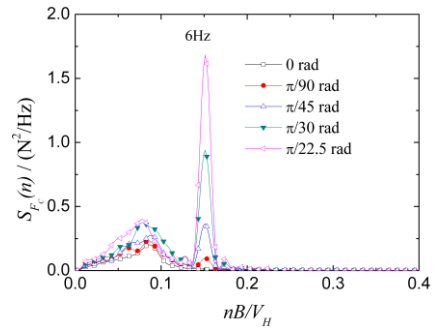
Fig. 13 Along-wind force spectra of Model 1

Fig. 14 Along-wind force spectra of Model 2

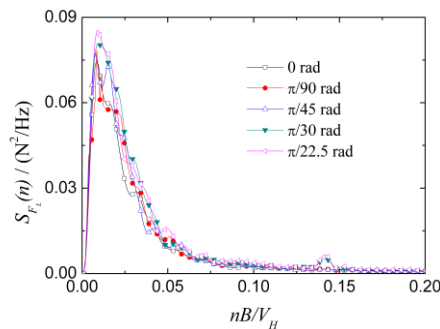
(3) The spectral peak values of both the torsional aerodynamic forces and the aeroelastic effects increase with the increase of the torsional vibration.



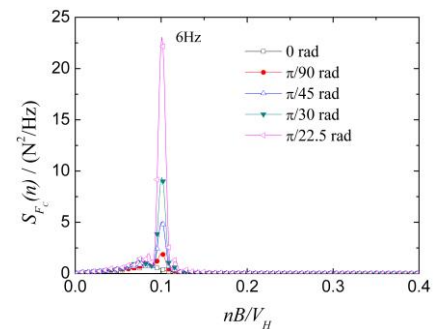
(a) $V_H/(n_0B)=9.4$



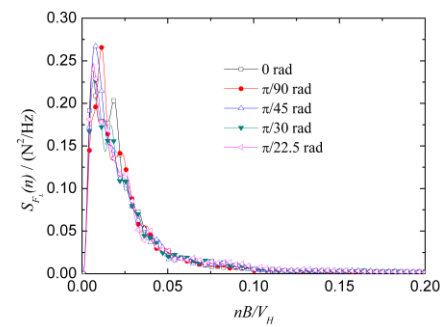
(a) $V_H/(n_0B)=6.7$



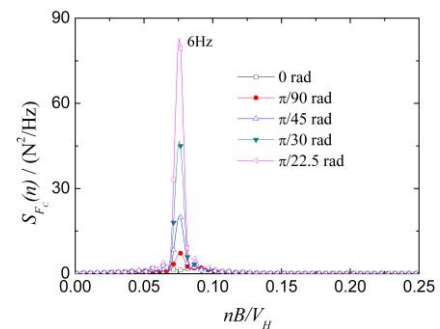
(b) $V_H/(n_0B)=14.2$



(b) $V_H/(n_0B)=10.0$



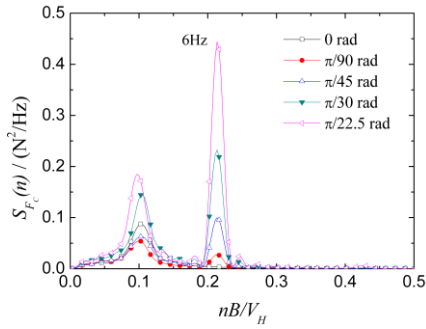
(c) $V_H/(n_0B)=18.9$



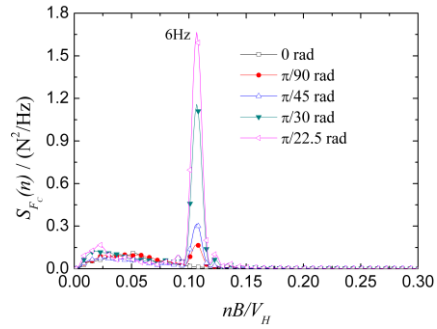
(c) $V_H/(n_0B)=13.3$

Fig. 15 Along-wind force spectra of Model 3

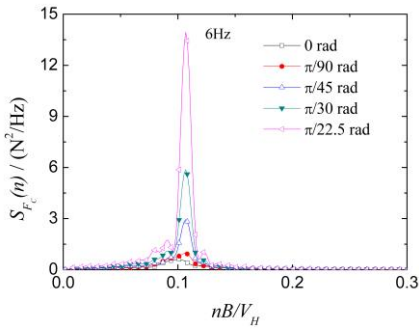
Fig. 16 Across-wind force spectra of Model 1



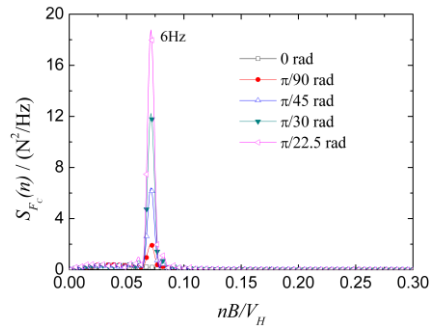
(a) $V_H/(n_0B)=4.7$



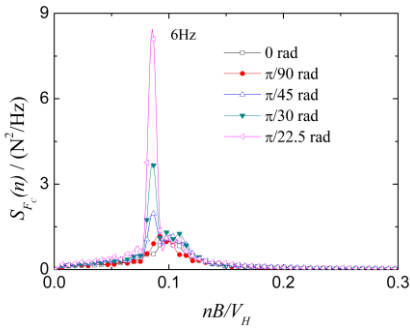
(a) $V_H/(n_0B)=9.4$



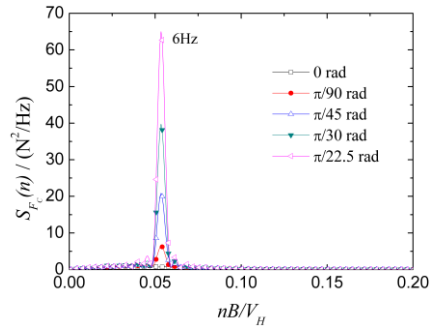
(b) $V_H/(n_0B)=9.4$



(b) $V_H/(n_0B)=14.2$



(c) $V_H/(n_0B)=11.8$



(c) $V_H/(n_0B)=18.9$

Fig. 17 Across-wind force spectra of Model 2

Fig. 18 Across-wind force spectra of Model 3

6. Conclusions

Generally speaking, the aerodynamic loads of tall buildings were obtained by wind tunnel tests of the static rigid model, and the aerodynamic damping was measured by aeroelastic model wind tunnel tests. However, the probably variation on the aerodynamic loads induced by the structural

vibration, and even the aerodynamic damping were neglected in the wind resistance design. The variation of the aerodynamic loads would cause the correspondence variation of wind-induced responses of tall buildings. The neglect of aeroelastic effects, especially the aerodynamic damping, would overestimate the wind-induced responses when the positive aerodynamic damping occurs and underestimate the responses with negative aerodynamic damping. Therefore, one significant error on evaluating structural dynamic responses might be due to the application of this type of aerodynamic loads with neglecting the aeroelastic effects. In order to analyze the effects of the structural torsional vibration on the aerodynamic loads and the aeroelastic effects of the tall buildings, a torsional motion-induced vibration device was designed to carry out the torsional vibration of the models in wind tunnel tests. By using this device, a very fine sinusoidal vibration in the torsional direction for the models was generated, which has a torsional fundamental constant type mode shape with a constant natural frequency. 3D aerodynamic loads of tall buildings were then measured by applying the device in the wind tunnel tests.

According to the RMS coefficients of the base shear/torque in the three directions, the effect of the torsional vibration and the reduced wind speeds on the aerodynamic loads are very significant when they are compared with the results measured by the wind tunnel tests on the rigid structural model. The RMS coefficients of the aerodynamic loads in the along-wind, across-wind, and torsional directions for the three studied models increase significantly with the increase of the torsional amplitudes. However the developing trends of the results in the along-wind, across-wind, and torsional directions with the reduced wind speeds are not the same. The RMS coefficients of the aerodynamic loads in the along-wind and torsional directions of the models decrease with the increase of the reduced wind speeds, while the RMS coefficients in the across-wind direction are more implicated. They have the characteristics of decreasing first, then increasing, and again decreasing with the increase of the reduced wind speeds, and they reach a maximum value under the critical wind speed of the vortex-excited resonance.

Theoretically, when the wind direction was perpendicular to the side B of the rectangular tall buildings, the wind loads in the along-wind and across-wind directions can be obtained by superposing the wind loads on the windward, leeward, and the two sideward facades, respectively. The wind loads in the torsional direction are derived from the contribution of the asymmetric wind pressures on the four facades. Therefore, it shows that the wind loads in the torsional direction are correlated to the wind loads in the along-wind and across-wind directions. In turn, when tall buildings oscillate in the torsional direction under strong wind actions, the wind flow characteristics (i.e., turbulence, attached flow, separation, and reattachment) around the buildings would be affected, which should result in considerable distinction of the dynamic wind pressures on the windward, leeward, and the sideward facades. This is the main reason that the torsional vibrations can enlarge the aerodynamic forces in the three directions as compared with the results measured on a static rigid model. Meanwhile, the effect of the torsional vibration on the aerodynamic forces in the three directions under the lower reduced wind speeds is much larger than that for higher reduced wind speeds. This is due to the fact that the torsional vibration plays a more important role in the wind-structure-interaction for a lower wind speed under given conditions that the structure has the same torsional vibration. In other words, the influence of the torsional vibration on the coupling effects of the structures and winds is more significant under a lower wind speeds.

In addition, the aeroelastic effects induced by the torsional vibration might be included in the along-wind, across-wind, and torsional directions due to the correlation of the wind loads in the torsional direction to the wind loads in the along-wind and across-wind directions. According to

the above analysis, the aerodynamic loads for the structure models in the three directions obtained by the torsional motion-induced vibration wind tunnel tests are identified to include two components (compared with the results for static rigid models): the aerodynamic forces and the aeroelastic effects. More details are obtained through the analysis of the spectra of the base shear/torque in the three directions.

The variation of the RMS coefficients of the aerodynamic loads in the along-wind direction is mainly determined by the aerodynamic forces but not by the aeroelastic effects. In addition, the variation of the RMS coefficients in the across-wind and torsional directions results from the increase of the aerodynamic forces and the aeroelastic effects due to the torsional vibration. In other words, both the torsional aeroelastic effects and the acrosswind aeoelastic effects are induced by the torsional vibration. Furthermore, the torsional vibration amplitudes and the reduced wind speeds are two critical parameters for the aerodynamic forces in the three directions as compared with the results for the rigid structural model.

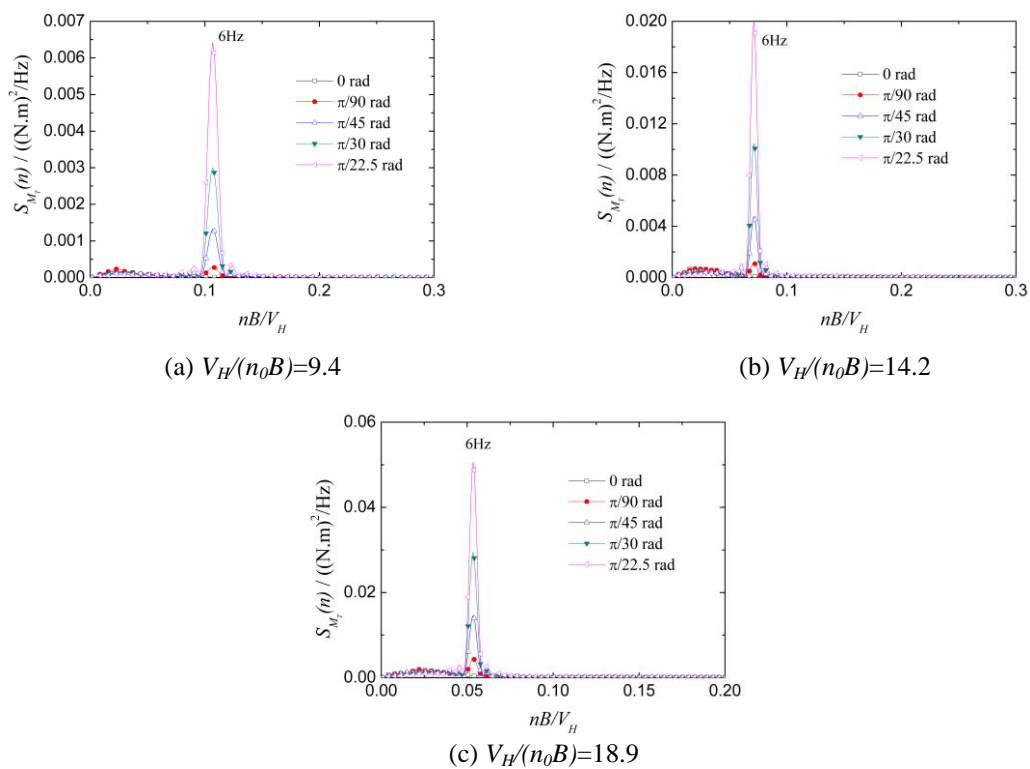


Fig. 21 Torsional force spectra of Model 3

For tall buildings, the emphasis of the structural wind-resistance design is to satisfy the comfortable requirements of the occupants, which means that the wind-induced acceleration responses should be limited within a predetermined value. In order to achieve a balance between the economics and the safety and serviceability in developing the structural wind resistance design of tall buildings, to obtain more accurate 3D aerodynamic loads of the tall buildings is of significant importance. The variation of the 3D RMS coefficients of the aerodynamic loads would result in the change of the 3D wind-induced responses and the equivalent static wind loads. Therefore, it is necessary to make certain corrections for the aerodynamic forces in the along-wind, across-wind, and torsional directions due to the torsional vibration, especially under the condition of large torsional vibration with strong wind loads. In addition, the aeroelastic effects, especially the aerodynamic damping, play an important role in the evaluation of the wind-induced dynamic responses of tall buildings. The wind-induced responses in different directions, when the aerodynamic damping in the corresponding direction is considered, might be different with the results that obtained through neglecting the aerodynamic damping. It is worth noting that the aeroelastic effects in both the torsional and acrosswind directions are induced by the torsional vibration. The contribution of the acrosswind aeroelastic effects induced by the torsional vibration on the acrosswind responses as well as the influence of the torsional aeroelastic effects to the torsional responses might be evaluated for the structural wind-resistant design. Finally, it should be noted that the aeroelastic effects of the structures in the across-wind direction induced by the torsional vibration have the same characteristic frequency as the torsional vibration. If the structural natural frequencies of tall buildings in the across-wind and torsional directions had a significant difference, the contribution of the across-wind aeroelastic effects induced by the torsional vibration to the valuation of the across-wind responses might be not distinctive. However, these effects need to be considered when the lowest torsional natural frequency approaches its lowest across-wind natural frequency.

Based on the observation and discussions of the experimental results obtained in this study, the main contributions are concluded as follows:

- The effects of the torsional vibration on the aerodynamic forces in the along-wind, across-wind, and torsional directions need to be considered. The torsional vibration amplitudes and the reduced wind speeds are two significant parameters to determine the variation of the aerodynamic forces in the three directions as compared with the results for the rigid structural models.
- The torsional vibration not only induces the aeroelastic effects in the torsional direction, but also induces the across-wind aeroelastic effects. The across-wind aeroelastic effects also need to be considered when the lowest torsional natural frequency approaches to its lowest across-wind natural frequency.

The limitations of the current study and future studies are as follows:

- Due to the limitations of the test facilities, using the constant torsional mode shape would result in certain error as compared to the real mode shape. For the 1st torsional mode of vibration, the angle of rotation would typically vary from 0 degrees at the base of the building to a maximum value at the top of the building. However, reliable results regarding torsional aeroelastic effects, including the torsional generalized aerodynamic forces measured by high frequency force balance, of tall buildings (similar torsional mode shape to that adopted in the current study) have ever been reported in the literature (Zhang *et al.* 1994, 1995). This error is thus not expected to impact the qualitative tendencies/rules in a major manner for the torsional

vibration on the 3D aerodynamic and aeroelastic forces of tall buildings, which can be served as basis for future studies.

The quantitative analysis of the change of the 3D aerodynamic forces and the torsional aeroelastic force (especially across-wind aeroelastic forces) induced by torsional vibration needs to be investigated.

Acknowledgments

The research presented in this paper was supported by the National Natural Science Foundation of China under project No. 51008240 and No. 51478369, which are gratefully acknowledged.

References

- Chan, C.M., Huang, M.F. and Kwok, K.C.S. (2010), "Integrated wind load analysis and stiffness optimization of tall buildings with 3D modes", *Eng. Struct.*, **32**(5), 1252-1261.
- Chen, X. and Kareem, A. (2005), "Coupled dynamic analysis and equivalent static wind loads on buildings with three-dimensional modes", *J. Struct. Eng. - ASCE*, **131**(7), 1071-1082.
- Chen, X.Z. (2013), "Estimation of stochastic acrosswind response of wind-excited tall buildings with nonlinear aerodynamic damping", *Eng. Struct.*, **56**, 766-778.
- Cheng, C.M., Lu, P.C. and Tsai, M.S. (2002), "Acrosswind aerodynamic damping of isolated square-shaped buildings", *J. Wind Eng. Ind. Aerod.*, **90**(12-15), 1743-1756.
- Cheung, J.C.K. and Melbourne, W.H. (1992), "Torsional moments of tall buildings", *J. Wind Eng. Ind. Aerod.*, **42**(1-3), 1125-1126.
- Choi, H. and Kanda, J. (1993), "Proposed formulae for the power spectrum of fluctuating lift and torque on rectangular 3-D cylinders", *J. Wind Eng. Ind. Aerod.*, **46-47**(8), 507-516.
- Elsharawy, M., Galal, K. and Stathopoulos, T. (2005), "Torsional and shear wind loads on flat-roofed buildings", *Eng. Struct.*, **84**, 313-324.
- Elsharawy, M., Galal, K. and Stathopoulos, T. (2014), "Design wind loads including torsion for rectangular buildings with horizontal aspect ratio of 1.6", *J. Struct. Eng. - ASCE*, **140**(4), 1-5.
- Elsharawy, M., Stathopoulos, T. and Galal, K. (2012), "Wind-induced torsional loads on low buildings", *J. Wind Eng. Ind. Aerod.*, **104**(SI), 40-48.
- GB50009-2012. (2012), "Wind loads for design of building structures", *China Architecture & Building Press*. (in Chinese)
- Gu, M. and Quan, Y. (2004), "Across-wind loads of typical tall buildings", *J. Wind Eng. Ind. Aerod.*, **92**(13), 1147-1165.
- Gu, M., Cao, H.L. and Quan, Y. (2014), "Experimental study of across-wind aerodynamic damping of super high-rise buildings with aerodynamically modified square cross-sections", *Struct. Des. Tall Spec. Build.*, **23**(16), 1225-1245.
- Islam, M.S., Ellingwood, B. and Corotis, R.B. (1992), "Wind-induced response of structurally asymmetric high-rise buildings", *J. Struct. Eng. - ASCE*, **118**(1), 207-222.
- Isyumov, N. and Case, P.C. (2000), "Wind-induced torsional loads and responses of buildings", *Proceedings of the structures congress, sponsored by ASCE/SEI*, Philadelphia, May.
- Kareem, A. (1992), "Dynamic response of high-rise buildings to stochastic wind loads", *J. Wind Eng. Ind. Aerod.*, **42**(1-3), 1101-1112.
- Keast, D.C., Barbagallo, A. and Wood, G.S. (2012), "Correlation of wind load combinations including torsion on medium-rise buildings", *Wind Struct.*, **15**(5), 423-439.
- Liang, S.G., Li, Q.S., Liu, S.C., Zhang, L.L. and Gu, M. (2004), "Torsional aerodynamic loads on

- rectangular tall buildings”, *Eng. Struct.*, **26**(1), 129-137.
- Liang, S.G., Liu, S.C., Li, Q.S., Zhang, L.L. and Gu, M. (2002), “Mathematical model of across wind dynamic loads on rectangular tall buildings”, *J. Wind Eng. Ind. Aerod.*, **90**(12-15), 1757-1770.
- Liang, S.G., Zou, L.H., Peng, X.H. and Chen, Z.Q. (2011), “Aerodynamic loads on tall building models undergoing bi-axial forced vibration in wind tunnel test”, *Proceedings of the 13th International Conference on Wind Engineering, Amsterdam*.
- Liang, S.G., Zou, L.H., Wang, D.H. and Huang, G.Q. (2014), “Analysis of three dimensional equivalent static wind loads of symmetric high-rise buildings based on wind tunnel tests”, *Wind Struct.*, **19**(5), 565-583.
- Marukawa, H., Kato, N., Fujii, K. and Tamura, Y. (1996), “Experimental evaluation of aerodynamic damping of tall buildings”, *J. Wind Eng. Ind. Aerod.*, **59**(2-3), 177-190.
- Marukawa, H., Ohkuma, T. and Momomura, Y. (1992), “Across-wind and torsional acceleration of prismatic high buildings”, *J. Wind Eng. Ind. Aerod.*, **42**(1-3), 1139-1150.
- Quan, Y., Gu, M. and Tamura, Y. (2005), “Experimental evaluation of aerodynamic damping of square super high-rise buildings”, *Wind Struct.*, **8**(5), 301-324.
- Solari, G. (1985), “Mathematical model to predict 3-D wind loading on buildings”, *J. Eng. Mech. - ASCE*, **111**(2), 254-275.
- Stekley, A. and Vickery, B.J. (1990), “On the measurement of motion-induced force on models in turbulent shear flow”, *J. Wind Eng. Ind. Aerod.*, **36**(1), 339-350.
- Tamura, Y., Kawai, H., Uematsu, Y., Marukawa, H., Fujii, K. and Taniike, Y. (1993), “Wind load and wind-induced response estimations in the recommendations for loads on buildings, AIJ 1993”, *Eng. Struct.*, **18**(6), 399-411.
- Tamura, Y., Kikuchi, H. and Hibi, K. (2008), “Peak normal stresses and effects of wind direction on wind load combinations for medium-rise buildings”, *J. Wind Eng. Ind. Aerod.*, **96**(6-7), 1043-1057.
- Vickery, B.J. and Stekley, A. (1993), “Aerodynamic damping and vortex excitation on an oscillating prism in turbulent shear flow”, *J. Wind Eng. Ind. Aerod.*, **49**(1-3), 121-140.
- Wu, J.C. and Chang, Y.C. (2009), “Along-wind aero-elasticity of prisms with different height/width ratios by indirect forced actuation technique”, *Proceedings of the 7th Asia-Pacific Conference on Wind Engineering, Chinese Taipei*.
- Zhang, W.J., Kwok, K.C.S. and Xu, Y.L. (1994), “Aeroelastic torsional behavior of tall buildings in wakes”, *J. Wind Eng. Ind. Aerod.*, **51**(2), 229-248.
- Zhang, W.J., Xu, Y.L. and Kwok, K.C.S. (1995), “Interference effects on eroelastic torsional response of structurally asymmetric tall buildings”, *J. Wind Eng. Ind. Aerod.*, **57**(1), 41-61.